Tryptophan 2,3-dioxygenase expression is prominent in human hepatocarcinoma cells, but is mostly restricted to pericytes in other human tumors

Delia Hoffmann[1,2], Tereza Dvorakova[1,2], Vincent Stroobant[1,2], Caroline Bouzin[3], Aurélie Daumerie[3], Marie Solvay[1,2], Simon Klaessens[1,2], Marie-Claire Letellier[4], Jean-Christophe Renauld[2], Nicolas van Baren[2], Julie Lelotte[5], Etienne Marbaix[2,5], Benoît Van den Eynde[1,2,6,*]

[1] Ludwig Institute for Cancer Research, Brussels B-1200, Belgium.
[2] de Duve Institute, UCLouvain, Brussels B-1200, Belgium.
[3] IREC Imaging Platform, Institut de Recherche Expérimentale et Clinique, UCLouvain, Brussels B-1200, Belgium.
[4] iTeos Therapeutics, Rue des Frères Wright 29, 6041 Gosselies, Belgium.
[5] Service d'anatomopathologie, Cliniques universitaires Saint-Luc, Brussels B-1200, Belgium
[6] Walloon Excellence in Life Sciences and Biotechnology, Brussels B-1200, Belgium.
* Correspondence and Lead Contact: Benoît Van den Eynde
Mailing address: Avenue Hippocrate, 75 B1.74.03 – B-1200 Brussels, BELGIUM
Phone number: 0032 2 764 75 72
Email address: benoit.vandeneynde@bru.licr.org

Running Title: TDO expression in human tumors

Keywords: Tryptophan 2,3-dioxygenase, tumor, placenta, pericyte, immunohistochemistry

Financial support for authors:

D. Hoffmann: FNRS-FRIA (Grant number: 1.E082.14)
T. Dvorakova: FNRS-Télévie (Grant number: 7.4597.18)
V. Stroobant: Ludwig Institute for Cancer Research
C. Bouzin: UCLouvain
A. Daumerie: UCLouvain
M. Solvay: FNRS-Aspirant (Grant number: 1.A385.16)
S. Klaessens: FNRS-FRIA (Grant number: 1.E100.14)
M.-C. Letellier: iTeos Therapeutics
J.-C. Renauld: UCLouvain
N. van Baren: de Duve Institute
J. Lelotte: Cliniques universitaires Saint-Luc
E. Marbaix: Cliniques universitaires Saint-Luc
B. Van den Eynde: Ludwig Institute for Cancer Research

Disclosure of Potential Conflicts of Interest:

M.-C.L. is employed by iTeos Therapeutics. B.V.d.E. is co-founder of, has ownership interest in, and SAB member of iTeos Therapeutics.

Abstract

Tryptophan catabolism is used by tumors to resist immune attack. It can be catalyzed by indoleamine 2,3-dioxygenase (IDO1) and tryptophan 2,3-dioxygenase (TDO). IDO1 is frequently expressed in tumors and has been widely studied as a potential therapeutic target to reduce resistance to cancer immunotherapy. In contrast, TDO expression in tumors is not well characterized. Several human tumor lines express enzymatically active TDO in a constitutive manner. In human tumor samples, TDO expression so far has been detected by transcriptomic studies, but the lack of validated antibodies has precluded detection of the TDO protein and identification of TDO-expressing cells. Here we develop novel TDO-specific monoclonal antibodies and confirm by immunohistochemistry the expression of TDO in the majority of human tumors. In all hepatocarcinomas, and in a few other tumors, TDO is expressed in tumor cells themselves. However, in the other tumors, TDO expression is restricted to pericytes, identified by their expression of PDGFRβ and their location in vascular structures. These TDO-expressing pericytes belong to morphologically abnormal tumor vessels and are found in high-grade tumors in the vicinity of necrotic or hemorrhagic areas, which are characterized by neoangiogenesis. We observed similar TDO-expressing pericytes in inflammatory pulmonary lesions containing granulation tissue, and in chorionic villi, two tissue types that also feature neoangiogenesis, suggesting a role for TDO in this process. Our results confirm TDO as a relevant immunotherapeutic target in hepatocellular carcinoma. In other tumor types, it is unclear at this stage whether TDO-expressing pericytes contribute to immunosuppression.

Introduction

Tryptophan catabolism is well described as one of the immunosuppressive mechanisms acting in the tumor microenvironment (1-3). Two distinct enzymes can convert tryptophan into kynurenine: indoleamine 2,3-dioxygenase 1 (IDO1) and tryptophan 2,3-dioxygenase (TDO protein or *TDO2* gene). Although both enzymes are located in the cytosol, their activity induces tryptophan depletion and kynurenine accumulation in the extracellular space, because of the action of amino-acid transporters (4-8). The concerted effects of tryptophan depletion and kynurenine accumulation make the microenvironment strongly immunosuppressive, reducing the proliferation of effector T lymphocytes and favoring the differentiation of regulatory T cells (9-12). In the steady state, the expression of IDO1 in normal tissues is restricted to endothelial cells in placenta and lung, mature dendritic cells and scattered epithelial cells in the female genital tract (13). However, IDO1 expression is massively induced in inflammatory sites following exposure to interferon gamma (IFNγ) (14,15). IDO1 induction in inflammatory sites is believed to contribute to the retro-control of T-cell responses, while placental IDO1 expression prevents immune rejection of the fetus by the maternal immune system (16). IDO1 is also expressed in many cancers and contributes to their resistance to immune rejection (1,13). Inflamed tumors can express IDO1 as an adaptive resistance mechanism, in which IDO1 is induced by the IFNγ produced by tumor-infiltrating T cells (17). However, a number of human tumors express IDO1 constitutively, as an intrinsic resistance mechanism that prevents T cell infiltration and may account for a number of cold tumors (18). This constitutive expression, which depends on oncogenic signaling through the MAPK and/or PI3K pathways, is exerted via COX2 inducing an autocrine loop of prostaglandin secretion, and can be repressed by clinically available COX2 inhibitors, thereby promoting tumor rejection (18). IDO1 activity can also be blocked by small molecule inhibitors, several of which are currently in clinical development (19). The most advanced IDO1 inhibitor, epacadostat, recently completed a Phase III clinical trial testing the combination of epacadostat with anti-PD1 pembrolizumab in

advanced melanoma (20). This trial showed no clinical benefit of the combination as compared to anti-PD1 alone. The potential reasons for this failure are numerous, but include a suboptimal dosing regimen and a lack of selection of tumors expressing IDO1 constitutively for inclusion in the trial. Another potential reason is the involvement of additional actors mediating tryptophan catabolism in the tumor microenvironment (21,22). The other main enzyme able to degrade tryptophan into kynurenine is TDO, which is expressed at a high level in the liver and degrades excess dietary tryptophan to maintain stable levels of systemic tryptophan (23). Its expression seems to be regulated in part by glucocorticoids (24) while TDO is post-translationally stabilized by its substrate (25,26). TDO expression was also detected in the decidualized endometrium, where its function is so far unknown (27-29), and in the brain where it might contribute to the synthesis of neuroactive compounds (30). TDO mRNA was also detected in a number of human tumor samples, including hepatocarcinomas but also glioblastomas, melanomas and bladder carcinomas (10,31). Expression of TDO in mouse tumors can prevent their immune rejection, and this effect can be reverted by systemic treatment of mice with a small-molecule inhibitor of TDO (31,32). These results prompted the preclinical and early clinical development of TDO inhibitors. Constitutive expression of TDO was observed in a number of human tumor lines, including glioblastoma lines and lines of colorectal, head & neck, lung and gall-bladder carcinomas (31). In those lines, TDO protein expression and activity was confirmed by enzymatic assays (31). In human tumor samples, TDO expression was detected by qRT-PCR but the lack of a reliable TDO-specific antibody prevented confirmation of protein expression as well as identification of the cell type(s) expressing TDO. These uncertainties have so far hampered clinical development of TDO inhibitors. In this report, using novel TDO-specific monoclonal antibodies, we confirm TDO protein expression in many human tumor samples, and identify the TDO-expressing cells in those samples.

Materials and methods

Production of TDO-specific mouse monoclonal antibodies

We immunized mice with cells expressing recombinant TDO at the cell surface as described (33). We made a pcDNA3 plasmid construct (ThermoFisher Scientific) encoding a fusion protein comprising human TDO at the C-terminal end of the type II transmembrane human CD134 ligand (hCD134L) protein. We immunized DBA/2 mice (purchased from Harlan Laboratories) with this plasmid 3 times at 2 weeks interval by electrotransfer of 20 µg DNA into the tibialis muscle. Two weeks after the last immunization, we boosted mice by injecting 10^5 living P1.HTR cells stably transfected with pCD.1-hCD134L-hTDO expression vector (33). These injections were performed in the footpad and repeated 3 times at 2-week intervals. P1.HTR cells were derived from the P815 mastocytoma cell line (34). Hybridomas were produced using standard procedures.

Mouse experiments

Animal studies were conducted in accordance with national and institutional guidelines for animal care and with the approval of the *Comité d'Ethique pour l'Expérimentation Animale* from the *Secteur des Sciences de la Santé*, UCLouvain (2011/UCL/MD/015 and 2015/UCL/MD/015).

Cancer cell lines

293-EBNA cells were purchased from InvivoGen. 293-EBNA transfected with human TDO cl119 were described (31). A172 (glioblastoma) was purchased from Antisense Pharma. Huh-7 (liver cancer) was a gift from A. Patel (Oxford). LB159-CRCA (colorectal carcinoma) was derived at the Ludwig Institute Brussels Branch from a patient sample in 1991 and cultured with homemade ACL-4 supplement. LB159-CRCA $TDO^{-/-}$ cells were generated using CRISPR/Cas9 as follows. Two different pairs of guide RNA (GR1-forward: CACCGTTTAAAAAACTCCCCGTAGA, GR1-reverse: AAACTCTACGGGGAGTTTTTTAAAC;

GR2-forward: CACCGGCAAAGGAGGTCTTATCTAT, GR2-reverse: AAACATAGATAAGACCTCCTTTGCC) were cloned into lentiCRISPR v2 plasmid (Addgene). LB159-CRCA cells were infected with both lentiviruses, selected with puromycin and cloned. The knockout of TDO was validated in clone 1 by DNA sequencing and by enzymatic assays (Fig. S1B). SK-CO-11 (colon cancer) and MZ-CHA-3 (gallbladder cancer) were received from collaborators in Mainz in 1991. LB1317-SCCHN (head and neck cancer) was derived at the Ludwig Institute Brussels Branch from a patient sample received from M. Hamoir and V. Grégoire (Cliniques universitaires Saint-Luc, Brussels) in 1996. U-87 MG (glioblastoma) was purchased from Cell Lines Service. To prepare FFPE cell pellets, cells were fixed for 20 minutes with 4% formaldehyde, washed with PBS, resuspended in 3% low-melting point agarose-PBS and embedded in paraffin using the Vacuum Infiltration Processor (Tissue-Tek).

Human tissues

Normal tissues and tumors were obtained from surgical resections or autopsies. The tissues used in this publication were provided by (i) the BioLibrary of the Institut Roi Albert II of the Cliniques universitaires Saint-Luc, Brussels, Belgium, projects CDCUCLR27 and CDCUCLR16-2016; (ii) the Service d'Anatomie Pathologique of the CHU-Brugmann, Brussels, Belgium; (iii) BHUL – Université de Liège – CHU de Liège, Belgium. The study was approved by the *Commission d'Ethique Biomédicale Hospitalo-Facultaire* from the UCLouvain (B403201316588) and conducted under the guidelines of the Helsinki declaration. Patients gave informed consent for the use of their tissues in this study.

Immunohistochemistry (IHC) an immunofluorescence (IF) multiplex stainings

Five µm-thick paraffin sections were deparaffinised and progressively rehydrated. Antigen retrieval was performed with Tris/EDTA buffer at pH 9 in a 2100 Antigen Retriever (Aptum). All the following steps were performed at room temperature. Endogenous peroxidases were blocked with Peroxidase Block (Dako) for 15 minutes and protein blocking was done for 1 hour with TBS-Tween containing 2% milk, 5% bovine serum albumin (biotin-free BSA) and 1%

human IgG. The primary antibodies (Table 1) were diluted in IHC diluent (Enzo) and incubated for 1 hour. After washing, the secondary antibodies (Table 1) were incubated for 1 hour. In case of IHC, the staining was revealed with HIGHDEF DAB substrate (Enzo) or with AEC+ Substrate Chromogen (Dako), counterstaining was done with hematoxylin and the slides were mounted with HIGHDEF IHC mount (Enzo). In case of multiplex IF, the staining was revealed with the Tyramide Signal Amplification (TSA) system (Table 1). Tyramide reagent was used at 1:50 in borate buffer. The antibodies were then eluted with citrate buffer at pH 6 using microwave treatment at 900 W until boiling followed by 15 minutes at 90 W. The following staining was started with protein blocking and pursued as described before. After the last staining, microwave treatment was performed, the nuclei were counterstained with Hoechst 33342 (Invitrogen) used at 20 µg/ml in TBS-Tween 0.1% with 10% BSA and the slides were mounted with HIGHDEF IHC fluoromount (Enzo). The slides were digitalized using a Pannoramic 250 Flash III tissue scanner (3DHISTECH) at x20 magnification. Multiplex-immunostained entire tumor sections were evaluated quantitatively using the image analysis tool Oncotopix version 2017.2 (Visiopharm).

In Situ Hybridization (ISH)

Five µm-thick paraffin sections were deparaffinised and progressively rehydrated. Endogenous peroxidases were blocked with RNAscope H2O2 (ACD) for 10 minutes at room temperature (RT). Antigen retrieval was performed with RNAscope Target Retrieval Reagents (ACD) for 15 minutes in a steam cooker. The slides were immediately transferred to water at RT, washed with ethanol and dried for several minutes up to overnight at RT. The slides were incubated with RNAscope Protease Plus (ACD) for 30 minutes at 40°C in a Dako Hybridizer. After washing with RNAscope Wash Buffer Reagents (ACD), the slides were incubated for 2 hours at 40°C with the primary probes: RNAscope Probe Hs-TDO2 (ACD, #416471), RNAscope Negative Control Probe dapB (ACD, #310043), RNAscope Hs-POLR2A (positive control, ACD, #310451). After extensive washing, the slides underwent incubation with 6 successive amplification probes from the revelation kit RNAscope 2.5 HD Detection Reagent

- BROWN (ACD, #322310) : AMP1 (30 min, 40°C), AMP2 (15 min, 40°C), AMP3 (30 min, 40°C), AMP4 (15 min, 40°C), AMP5 (30 min, RT), AMP6 (15 min, RT). The staining was revealed with DAB from the same kit for 10 minutes at RT. Counter-staining was done with hematoxylin and the slides were mounted with HIGHDEF IHC mount (Enzo).

Quantitative RT-PCR

RNA of frozen cells and tissues was extracted with NucleoSpin RNA (Macherey Nagel) according to the manufacturer's instructions. Whole tissues were beforehand crushed in the lysis buffer of the kit using a TissueLyser LT (Qiagen). RNA of FFPE tissue sections was extracted with NucleoSpin total RNA FFPE XS (Macherey Nagel) according to the manufacturer's instructions. A defined amount of RNA was retro-transcribed by the RevertAid RT Kit (ThermoFisher Scientific). qPCR was performed with Takyon ROX Probe 2X MasterMix dTTP blue (Eurogentec) in a StepOnePlus thermal cycler (Applied Biosystems) using the following program for human *IDO1*, human and murine *TDO2*: 3 minutes at 95°C, then 40 cycles of 10 seconds at 95°C and 1 minute at 60°C; for human *EF1* and murine *β-actin*: 3 minutes at 95°C, then 40 cycles of 3 seconds at 95°C and 30 seconds at 60°C. The following primers were used (F = forward, R = reverse, P = probe):

hIDO1:

F 5'-GGTCATGGAGATGTCCGTAA-3'

R 5'-ACCAATAGAGAGACCAGGAAGAA-3'

P 5'-CTGTTCCTTACTGCCAACTCTCCAAGAAACTG-3'

hTDO2:

F 5'-CATGGCTGGAAAGAACTC-3'

R 5'-CTGAAGTGCTCTGTATGAC-3'

P 5'-TTTAGAGCCACATGGATTTAACTTCTGGG-3'

hEF1:

F 5'-GCTTCACTGCTCAGGTGAT-3'

R 5'-GCCGTGTGGCAATCCAAT-3'

P 5'-AAATAAGCGCCGGCTATGCCCCTG-3'

mTDO2:

F 5'-GTATCTATGGAGGACAATGAAG-3'

R 5'-GATGAATAGGTGCTCGTCATG-3'

P 5'-CCTCCTTTGCTGGCTCTGTTTACACC-3'

mβ-actin:

F 5'-CTCTGGCTCCTAGCACCATGAAG-3'

R 5'-GCTGGAAGGTGGACAGTGAG-3'

P 5'-ATCGGTGGCTCCATCCTGGC-3'

The probes were coupled to 5' FAM and 3' TAMRA. Standard curves were added for each gene.

Tryptophan and kynurenine quantification

The culture supernatants were analyzed by HPLC as previously described (31).

Western blot (WB)

Protocol #1: The cells and whole livers were lysed in Pierce Ripa buffer (ThermoFisher Scientific) with Halt Protease and Phosphatase Inhibitor Cocktail (ThermoFisher Scientific). The livers were crushed using a TissueLyser LT (Quiagen). A defined amount of proteins was heated at 95°C for 5 minutes with Laemmli loading buffer. 20 µg of proteins were loaded on NuPAGE Bis Tris 4-12% gels (ThermoFisher Scientific) and separated by gel electrophoresis using NuPAGE MOPS SDS Running Buffer (ThermoFisher Scientific). Dry transfer was performed by iBlot (ThermoFisher Scientific) using iBlot Gel Transfer Stacks, nitrocellulose, regular size (ThermoFisher Scientific) and a transfer program of 7 minutes (1 minute at 20 V, 4 minutes at 23 V, 2 minutes at 25 V). After blocking, the membranes were incubated for 2 hours at room temperature with the primary antibodies: mouse anti-TDO clone III at 1 µg/ml, clone V at 1 µg/ml or mouse anti-Vinculin clone hVIN-1 at 1:10,000 (Sigma-Aldrich, #V9131). After washing, the membranes were incubated with HRP-linked goat anti-mouse IgG antibody

(BioLegend, #405306) at 1:2,500 in blocking buffer for 1 hour at room temperature and washed again. HRP was revealed using SuperSignal West Pico (ThermoFisher Scientific) and detected with Fusion Solo S (Vilber Lourmat).

Protocol #2: The cells were lysed in a homemade lysis buffer (0.1% SDS, 1% sodium deoxycholate, 0.5% Nonidet P40) with cOmplete Protease Inhibitor Cocktail (Sigma-Aldrich). A defined amount of proteins was heated with NuPAGE LDS Sample Buffer (ThermoFisher Scientific) and NuPAGE Sample Reducing Agent (ThermoFisher Scientific). 20 µg of proteins were loaded on Bolt 4-12% Bis-Tris Plus Gels (ThermoFisher Scientific) and separated by gel electrophoresis using Bolt MOPS SDS Running Buffer (ThermoFisher Scientific). Dry transfer was performed like in protocol #1. The membranes were incubated overnight at 4°C with the primary antibodies: mouse anti-TDO clone III at 1 µg/ml, clone V at 1 µg/ml or mouse anti-β-actin clone AC-15 at 1:10,000 (Sigma-Aldrich, #A5441). After washing, the membranes were incubated with HRP-linked goat anti-mouse IgG antibody (R&D systems, #HAF007) at 1:5,000 for 1 hour at room temperature and washed again. HRP was revealed like in protocol #1. TDO and β-actin were stained on the same membrane and stripping between both stainings was performed by 15 minutes incubation in Restore PLUS Western Blot Stripping Buffer (ThermoFisher Scientific).

Results

Production and validation of TDO-specific antibodies

Given the lack of fully validated antibodies recognizing TDO, we first produced new TDO-specific monoclonal antibodies by immunizing mice with DNA and boosting with cells engineered to express full-length human TDO at the cell surface (33). We selected two clones (clone V, IgG2aκ, and clone III, IgG2bκ) and validated them based on the following criteria. They recognized a single band of the expected size (47kDa) only in human cell lines that express TDO mRNA (Fig. S1A). This band disappeared after CRISPR-Cas9 genetic inactivation of TDO (Fig. S1B). In TDO-negative human cells, the same band appeared upon transfection of TDO (Fig. S1B). This band was absent in cells expressing IDO1 but not TDO, indicating specificity (Fig. S1A). While both mAbs recognized human TDO, only mAb V recognized mouse TDO, and stained a single band in liver lysates from WT but not from $TDO^{-/-}$ mice (Fig. S1C). Of note, human and murine TDO are 89% identical. Immunohistochemistry (IHC) of fixed pellets of human cells showed a cytoplasmic staining in cell lines expressing TDO but not in TDO-negative cell lines (Fig. S1D).

TDO is expressed in the majority of late stage human tumors

We then used these antibodies to analyze the expression of TDO in human tumors and determine the proportion and the type of cells that express TDO. We stained a large number of human tumors of various histologies with both mAbs and found TDO-positive cells in most of them (Fig. 1A and Table 2). The results obtained with both TDO mAbs were identical. Importantly, in all cases we used adjacent sections to detect the presence of TDO mRNA by RT-qPCR and/or in situ hybridization (ISH) to validate the specificity of the stainings (Fig. 1B). Samples were only considered positive when they were stained by IHC with both antibodies and contained *TDO2* mRNA.

With the exception of astrocytomas, we found TDO-positive samples in all tumor types. All hepatocarcinomas expressed TDO and showed cytoplasmic staining in most tumor cells (Fig. 1A). This is in line with the physiological expression of TDO in normal hepatocytes. Other tumors, including glioblastomas, bladder, pancreatic and colon carcinomas, also showed a high proportion of TDO-positive samples, but here the staining was limited to some cells in restricted tumor areas. A similar staining pattern was observed in all the other TDO-positive tumors (Fig. 1A, Table 2). Interestingly, although only half of the melanomas and breast carcinomas were positive, more than 80% of the corresponding metastatic lymph nodes contained TDO-expressing cells, which were absent from non-metastatic lymph nodes (Table 2).

These restricted tumor areas expressing TDO appeared to correspond to vascular structures, which were often located at the tumor periphery or surrounded necrotic and hemorrhagic areas (Fig. 1A). In tumor-infiltrated lymph nodes, they were mainly found at the borders of the metastases and at the interface between tumor and lymphatic tissue. We then wondered whether the level of TDO expression was correlated with clinical features, such as the age of the patients, their treatment, the tumor grade, and the presence of lymph node or distant metastases. Considering all tumor types (except hepatocarcinomas) we found that the proportion of TDO-expressing cells was inversely correlated with tumor differentiation, with higher proportions in higher histological grades (Fig. 1C). An illustrative example is glioma: while grade II and III astrocytomas were all TDO-negative, 97% of glioblastomas multiforme (grade IV gliomas) contained TDO-positive cells (Table 2).

TDO is expressed in human tumors by morphologically abnormal vessels

To identify the cell type expressing TDO in these vascular structures, we performed a series of co-stainings (Fig. 2A). We observed that all TDO-positive cells expressed the beta-type platelet-derived growth factor receptor (PDGFRβ), a marker of mesenchymal cells (fibroblasts,

328 pericytes, vascular smooth muscle cells (vSMCs)), while not all PDGFRβ-positive cells
329 expressed TDO. Some, but not all, TDO-positive cells expressed α-smooth muscle actin
330 (αSMA) and NG2 (neural/glial antigen 2). TDO-positive cells also surrounded CD34-positive
331 endothelial cells, but TDO never co-localized with CD34. We therefore concluded that TDO-
332 expressing cells corresponded to vascular smooth muscle cells or pericytes. These two cell
333 types, which have very similar phenotypes, can be identified according to their localization
334 towards the basement membrane in normal vessels, but can no longer be distinguished in
335 disorganized tumor vessels (35,36). In addition to TDO-positive pericytes, which were
336 identified in all tumor types including hepatocellular carcinomas, some tumors also contained
337 TDO-expressing tumor cells, including, as mentioned above, all hepatocellular carcinomas,
338 but also 10/39 glioblastomas, in which TDO was partially co-expressed with GFAP and β3-
339 tubulin (Fig. 2A), and 1/10 kidney carcinoma (Fig. 1B). Those TDO-positive tumor cells
340 surrounded TDO-positive vessels bordering necrotic tumor areas. In none of the tested tumors,
341 TDO was expressed by macrophages or dendritic cells (HLA-DR-positive) (Fig. 2A).
342
343 Although most tumors contained TDO-positive cells, those cells were numerically poorly
344 represented. In 34 analyzed glioblastomas multiforme, the tumor type with the highest amount
345 of TDO-expressing pericytes, only 5.9% of the PDGFRβ-stained area was also positive for
346 TDO (workflow described in Fig. S2). We used PDGFRβ rather than αSMA or NG2 as a
347 pericyte marker, because not all TDO-positive cells expressed αSMA or NG2. However,
348 glioblastomas also contained a few PDGFRβ-positive fibroblasts that were TDO-negative.
349 Therefore, 5.9% is probably a slight underestimation of the proportion of TDO-positive
350 pericytes.
351
352 TDO-positive tumor vessels often displayed abnormal features, that were similar to the
353 vascular anomalies previously observed in tumors (36). These included accumulation of little
354 vessels surrounded by several layers of pericytes (Fig. 2B, 1st line), and enlarged vessels with
355 a single, irregular layer of pericytes (Fig. 2B, 2nd line). We also found normal TDO-positive

capillaries, but they were much less abundant (Fig. 2B, 3rd line). We therefore wondered whether TDO-positive vessels were well perfused or whether those tumor areas were hypoxic. We found no co-staining of TDO with the hypoxia marker carbonic anhydrase 9 (CA9). This result suggested that TDO-positive tumor regions were well oxygenated, but did not exclude blood and oxygen supply by neighboring TDO-negative vessels (Fig. 2C).

TDO and IDO1 do not co-localize in glioblastomas

We wondered if TDO co-localized with IDO1, the other tryptophan-metabolizing enzyme. Immunohistochemistry stainings of glioblastoma multiforme showed that IDO1 was expressed by very few cells, which were either tumor cells or cells with a dendritic cell-like shape (Fig. S3A). Co-stainings with TDO were performed on 5 tumors and showed that both proteins never co-localized (Fig. S3B).

TDO does not impact the infiltration of lymphocytes in glioblastomas

In mouse tumor models, we previously described the immunosuppressive role of TDO when expressed homogeneously by tumor cells (31). This situation is nicely reflected in human hepatocarcinomas, which homogeneously express TDO in tumor cells. It was unclear, however, whether the low proportion of TDO-expressing vascular cells we observed in other tumors would suffice to catabolize tryptophan in a meaningful immunosuppressive way. This was difficult to address in mouse models, in which we never observed a similar expression of TDO in tumor vessels (37). To try to address this question, we co-stained 29 human glioblastomas for T lymphocytes (CD3 and CD8) and TDO, and used an image analysis algorithm to quantify lymphocyte infiltration in TDO-positive versus TDO-negative tumor areas (workflow described in Fig. S4). Glioblastomas have the advantage that they rarely express IDO1 (13) (Fig. S3). As expected, T cell infiltration was low in these glioblastomas (38). Tumor regions within 60 µm of a TDO-expressing cell (whether a pericyte or a tumor cell) contained slightly more – not less – CD3-expressing lymphocytes, whether or not they also expressed CD8 (Fig. 3A and S4). Moreover, T lymphocytes present in TDO-positive areas tended to be

more proliferative, as indicated by Ki67 staining (Fig. 3B and S4). These results suggest that the presence of TDO-positive pericytes does not prevent but might instead favor lymphocyte infiltration in glioblastoma, although this enrichment might result from the fact that the TDO-positive areas were close to vessels, while the TDO-negative areas we used for comparison were not, for technical reasons, selected to be close to vessels. Although our approach did not assess lymphocyte function or differentiation, these data do not support an important immunosuppressive role of TDO-expressing pericytes in the tumor microenvironment.

TDO expression in pericytes from inflammatory pulmonary lesions

We then took advantage of our validated TDO-specific mAb to evaluate the expression profile of TDO in normal tissues. We stained non-tumoral sections from the organs harboring the tumors listed in Table 2, including 5 pancreata, 1 uterus, 3 colons, 2 stomachs, 2 lungs, 6 kidneys, 10 livers and 10 bladders. Those tissues were negative for TDO, with the exception of liver and lung. As expected, all liver samples showed TDO expression in hepatocytes (Fig. 4A).

Unexpectedly, both lung samples contained TDO-positive pericytes. To determine whether TDO expression was linked to the presence of a tumor in the lung, we stained 11 additional non-tumoral lung samples collected at a distance from the lesion in patients with or without benign or malignant tumor, as indicated in Table 3. Five of them contained TDO-expressing pericytes (Fig. 4A, B). Interestingly, all 7 samples containing TDO-positive cells also showed signs of inflammation, some of them also containing granulation tissue (Table 3). In contrast, none of the six samples without inflammation contained TDO-expressing vessels (Table 3). These results indicated that TDO expression in lung pericytes was associated with inflammatory processes.

TDO expression in decidua and placenta

411 Because the murine decidua is known to express TDO (27-29), we also tested human deciduas
412 of the first trimester and ectopic pregnancies by IHC. We only found TDO expression in a few
413 cells, which corresponded to pericytes (PDGFRβ-positive) located inside chorionic villi, and to
414 interstitial syncytiotrophoblasts (multinuclear cells expressing cytokeratin) (Fig. 4A, B).

Discussion

So far, the evidence supporting TDO expression in human tumors was threefold. First, *TDO2* mRNA was detected in human tumors by RT-qPCR performed on bulk tumor RNA (31). Second, a number of human tumor lines were found to express TDO at the mRNA and protein level, and to effectively degrade tryptophan into kynurenine, in a manner that was inhibited by TDO inhibitors (10,31). Third, IHC studies performed on several human tumor types (colon carcinoma, breast cancer, non-small cell lung carcinoma, ovarian carcinoma, renal cell carcinoma and brain metastases of malignant melanoma) reported widespread and homogeneous expression of TDO in tumor cells (10). Based on the expression of TDO in human tumor lines and on the staining patterns reported by Opitz et al, it was considered that TDO was expressed by tumor cells themselves in human tumors. However, no validated TDO-specific monoclonal antibody was available at the time, so that the reported IHC stainings were performed with non-validated polyclonal antibodies, which carry the inherent risk of cross reactivity, particularly when used for IHC, which does not control for the molecular size of the signal. In this study, we describe and fully validate two highly specific monoclonal antibodies recognizing TDO. They stain a single band of the expected molecular weight when used in western blots, and score positive in both western blot and IHC on cell lines genetically controlled to express TDO, while they are totally negative in cell lines with a silent or a CRISPR-deleted TDO gene. Using these mAb, we confirmed TDO expression in a large number of human tumors. In hepatocellular carcinoma (HCC), TDO was highly expressed in tumor cells themselves. In other tumors however, we did not observe TDO expression in tumor cells, but only in scattered cells often located next to necrotic or hemorrhagic areas. The TDO specificity of this staining was further confirmed by *in situ* hybridization, which detected a similar expression pattern of TDO mRNA in adjacent sections. TDO-expressing cells belonged to vascular structures with abnormal morphology, typical of vascular anomalies previously reported in tumor vessels (36). Further stainings identified these TDO-expressing cells as pericytes/vSMCs, expressing PDGFRβ. This result came as a surprise, particularly given the

443 expression of TDO in several human tumor lines of glioblastoma and carcinoma of the colon,
444 head and neck, lung and gallbladder (10,31). This disconnection between tumor lines and
445 tumor samples is intriguing, even more so when considering human HCC, in which the
446 opposite disconnection is observed: although TDO is expressed in tumor cells in HCC
447 samples, HCC lines tested so far proved negative for TDO expression (31).
448
449 The function of hepatic TDO is to regulate systemic tryptophan concentrations, as illustrated
450 by the 9-fold increased level of tryptophan in the serum of TDO-KO mice (23,37). By analogy
451 to the tryptophan-degrading enzyme IDO1, the proposed function of TDO in tumors is the
452 inhibition of immune-mediated tumor rejection. The impact of IDO1 on immune evasion has
453 been extensively studied in *in vivo* experiments using different tumor models (1,18,39,40). In
454 humans, IDO1 is expressed by a large number of tumors and high IDO1 expression is
455 positively correlated with tumor progression and decreased survival (2,19,41). Several IDO1
456 inhibitors are now in clinical development (19). Similar to IDO1, TDO was shown in several *in*
457 *vitro* and *in vivo* experiments to negatively impact T lymphocyte activity and proliferation. TDO-
458 positive cells block *in vitro* IFNγ production and proliferation of T lymphocytes (42) and TDO
459 favors escape of murine tumors to immune rejection (31). The outcome of LPS-induced
460 endotoxemia is worsened in $TDO^{-/-}$ mice due to the increased secretion of pro-inflammatory
461 cytokines (43). The dominant expression of TDO in human HCC confirms the potential of TDO
462 as a therapeutic target in this cancer type. Although checkpoint inhibitors were recently
463 approved in HCC (44,45), their clinical efficacy remains limited and could be improved upon
464 combination with TDO inhibitors, several of which have been developed (31,32,37,46).
465
466 In other tumor types, the role of TDO expression in pericytes associated with abnormal tumor
467 vessels is unclear at this stage. A local immunosuppressive function is possible and in line with
468 previous reports indicating that tumor-derived vascular pericytes can anergize Th cells (47).
469 Moreover, pericytes derived from human glioblastomas were found to have stem cell-like and
470 immunosuppressive properties, associated with TDO expression which, however, was very

low in the experimental conditions used (48). Because we could not find expression of TDO in murine tumor-associated pericytes, we could not experimentally test the immunosuppressive role of TDO-expressing pericytes *in vivo* (37). In human glioblastoma, our quantification of T cells in tumor areas containing TDO-positive cells did not show a reduced infiltration or proliferation of CD3- or CD8-positive cells. This result suggests that TDO-expressing pericytes do not negatively affect the recruitment and infiltration of T cells into the tumor, while they can still affect the functional status or anergic state of tumor-infiltrating lymphocytes. However, although present in most tumor samples, TDO-expressing pericytes populate only about 6% of tumor vessels within a given sample. It is unclear whether such a low proportion of TDO-expressing cells suffices to induce the level of tryptophan degradation that is required to induce immunosuppression in the whole tumor mass.

We observed that TDO-positive vessels were often located around necrotic and hemorrhagic tumor areas, which are characterized by neovascularization. We also found TDO-expressing vessels in non-tumoral lung granulation tissue, which also involves neovascularization, and in chorionic villi at the time of embryonic vessel formation. TDO could therefore play a role in neovascularization, for example through the vasoactive function of one of the tryptophan-derived metabolites. Kynurenine produced by endothelial cells expressing IDO1 during inflammation can induce vessel relaxation, and the severity of septic shock is directly correlated to the expression of IDO1 (49,50). In addition, a newly described tryptophan-derived tricyclic hydroperoxide, formed by IDO1 in the presence of H_2O_2, causes vessel relaxation of IFNγ-pretreated mouse abdominal aortas (51). This or a similar compound could be also produced by TDO, given the similar enzymatic mechanism of both enzymes. A link between TDO expression and neovascularization would also be in line with our observation that glioblastomas, which display much more neoangiogenesis as compared to astrocytomas, also contain much more TDO-expressing vessels (Table 2).

An interesting question is the mechanism that triggers TDO expression in tumor pericytes. Rat hepatocytes increase *TDO2* expression upon treatment with glucocorticoids (24) whereas murine decidual cells do so upon exposure to estrogen and progesterone (29). We treated murine mesenchymal stem cells (MSC) or MSCs differentiated to fibroblasts/vSMCs with dexamethasone, different combinations of pregnancy hormones or cytokines, but we could not detect any induction of *TDO2* mRNA (Table S1). As TDO is expressed in the murine decidua, the maternal part of the placenta (28,29), we also treated decidualized and undecidualized uterine cells. Except for a small increase of TDO expression by LPS and IFNγ in decidualized cells, TDO could not be induced (Table S1). As we observed TDO-positive pericytes in angiogenic tumor areas, granuloma tissues and in placenta, the induction of TDO might result from a complex interplay of different physiological and pathological phenomena related to hypoxia and inflammation. In line with this, recent reports described the induction of TDO in fibroblasts, which, like pericytes, are derived from mesenchymal stem cells: TDO was up-regulated in uterine stromal fibroblasts by natural killer cells (52) and in normal lung fibroblasts by galectin-1 secreted from lung tumor cell lines (53).

In sum, our results confirm TDO expression at the protein level in a large range of human tumors. The high TDO expression by HCC cells clearly warrants the development of TDO inhibitors in this indication. In other cancer indications, TDO inhibitors may synergize with immunotherapy in a different manner, by blocking hepatic TDO and increasing systemic tryptophan levels, as we report in the accompanying manuscript (37).

Acknowledgements

We thank Dr Hiroshi Funakoshi, Dr Toshikazu Nakamura and Pr Michael Platten for providing TDO-KO mice; Guy Warnier and his team for the production of TDO-KO mice; the BioLibrary of the Institut Roi Albert II of the Cliniques universitaires Saint-Luc (Brussels, Belgium), the Service d'Anatomie Pathologique of the CHU-Brugmann (Brussels, Belgium), BHUL – Université de Liège – CHU de Liège (Belgium) and Prof Christine Galant for providing tissue samples; Vanesa Bol for the ISH protocol; and Auriane Sibille for editorial assistance.

Funding

This work was supported by Ludwig Cancer Research, the Fonds Scientifique pour la Recherche – FNRS, de Duve Institute and UCLouvain (Belgium).

Author Contributions

Conception and design: D.H. and B.V.d.E.

Methodology: D.H. and B.V.d.E.

Acquisition of data: D.H., T.D., V.S., C.B., A.D., M.S., S.K., M.-C.L., J.-C.R., N.v.B., J.L., E.M.

Writing – Original Draft: D.H. and B.V.d.E.

Study supervision: B.V.d.E.

Bibliography

1. Uyttenhove C, Pilotte L, Theate I, Stroobant V, Colau D, Parmentier N*, et al.* Evidence for a tumoral immune resistance mechanism based on tryptophan degradation by indoleamine 2,3-dioxygenase. *Nat Med* **2003**;9(10):1269-74.
2. van Baren N, Van den Eynde BJ. Tryptophan-degrading enzymes in tumoral immune resistance. *Front Immunol* **2015**;6:34.
3. van Baren N, Van den Eynde BJ. Tumoral Immune Resistance Mediated by Enzymes That Degrade Tryptophan. *Cancer Immunol Res* **2015**;3(9):978-85.
4. Oxender DL, Christensen HN. Evidence for two types of mediation of neutral and amino-acid transport in Ehrlich cells. *Nature* **1963**;197:765-7.
5. Vumma R, Johansson J, Lewander T, Venizelos N. Tryptophan transport in human fibroblast cells-a functional characterization. *Int J Tryptophan Res* **2011**;4:19-27.
6. Kudo Y, Boyd CA. Characterisation of L-tryptophan transporters in human placenta: a comparison of brush border and basal membrane vesicles. *J Physiol* **2001**;531(Pt 2):405-516.
7. Kaper T, Looger LL, Takanaga H, Platten M, Steinman L, Frommer WB. Nanosensor detection of an immunoregulatory tryptophan influx/kynurenine efflux cycle. *PLoS Biol* **2007**;5(10):e257.
8. Speciale C, Hares K, Schwarcz R, Brookes N. High-affinity uptake of L-kynurenine by a Na+-independent transporter of neutral amino acids in astrocytes. *J Neurosci* **1989**;9(6):2066-72.
9. Munn DH, Sharma MD, Baban B, Harding HP, Zhang Y, Ron D*, et al.* GCN2 kinase in T cells mediates proliferative arrest and anergy induction in response to indoleamine 2,3-dioxygenase. *Immunity* **2005**;22(5):633-42.
10. Opitz CA, Litzenburger UM, Sahm F, Ott M, Tritschler I, Trump S*, et al.* An endogenous tumour-promoting ligand of the human aryl hydrocarbon receptor. *Nature* **2011**;478(7368):197-203.
11. Terness P, Bauer TM, Rose L, Dufter C, Watzlik A, Simon H*, et al.* Inhibition of allogeneic T cell proliferation by indoleamine 2,3-dioxygenase-expressing dendritic cells: mediation of suppression by tryptophan metabolites. *J Exp Med* **2002**;196(4):447-57.
12. Mezrich JD, Fechner JH, Zhang X, Johnson BP, Burlingham WJ, Bradfield CA. An interaction between kynurenine and the aryl hydrocarbon receptor can generate regulatory T cells. *J Immunol* **2010**;185(6):3190-8.
13. Theate I, van Baren N, Pilotte L, Moulin P, Larrieu P, Renauld JC*, et al.* Extensive profiling of the expression of the indoleamine 2,3-dioxygenase 1 protein in normal and tumoral human tissues. *Cancer Immunol Res* **2015**;3(2):161-72.
14. Dai W, Gupta SL. Regulation of indoleamine 2,3-dioxygenase gene expression in human fibroblasts by interferon-gamma. Upstream control region discriminates between interferon-gamma and interferon-alpha. *J Biol Chem* **1990**;265(32):19871-1987.
15. Chon SY, Hassanain HH, Pine R, Gupta SL. Involvement of two regulatory elements in interferon-gamma-regulated expression of human indoleamine 2,3-dioxygenase gene. *J Interferon Cytokine Res* **1995**;15(6):517-26.
16. Munn DH, Zhou M, Attwood JT, Bondarev I, Conway SJ, Marshall B*, et al.* Prevention of allogeneic fetal rejection by tryptophan catabolism. *Science* **1998**;281(5380):1191-3.
17. Spranger S, Spaapen RM, Zha Y, Williams J, Meng Y, Ha TT*, et al.* Up-regulation of PD-L1, IDO, and T(regs) in the melanoma tumor microenvironment is driven by CD8(+) T cells. *Sci Transl Med* **2013**;5(200):200ra116.
18. Hennequart M, Pilotte L, Cane S, Hoffmann D, Stroobant V, De Plaen E*, et al.* Constitutive IDO1 Expression in Human Tumors Is Driven by Cyclooxygenase-2 and Mediates Intrinsic Immune Resistance. *Cancer Immunol Res* **2017**;5(8):695-709.
19. Brochez L, Chevolet I, Kruse V. The rationale of indoleamine 2,3-dioxygenase inhibition for cancer therapy. *Eur J Cancer* **2017**;76:167-82.
20. Long GV, Dummer R, Hamid O, Gajewski T, Caglevic C, Dalle S*, et al.* Epacadostat (E) plus pembrolizumab (P) versus pembrolizumab alone in patients (pts) with unresectable or

metastatic melanoma: Results of the phase 3 ECHO-301/KEYNOTE-252 study. *Journal of Clinical Oncology* **2018**;36(15_suppl):108-.
21. Van den Eynde BJ, van Baren N, Baurain JF. Is there a clinical future for IDO1 inhibitors after the failure of epacadostat in melanoma? *Annu Rev Cancer Biol* **2019**;4(In press).
22. Muller AJ, Manfredi MG, Zakharia Y, Prendergast GC. Inhibiting IDO pathways to treat cancer: lessons from the ECHO-301 trial and beyond. *Semin Immunopathol* **2019**;41(1):41-8.
23. Kanai M, Funakoshi H, Takahashi H, Hayakawa T, Mizuno S, Matsumoto K*, et al.* Tryptophan 2,3-dioxygenase is a key modulator of physiological neurogenesis and anxiety-related behavior in mice. *Mol Brain* **2009**;2:8.
24. Danesch U, Hashimoto S, Renkawitz R, Schutz G. Transcriptional regulation of the tryptophan oxygenase gene in rat liver by glucocorticoids. *J Biol Chem* **1983**;258(8):4750-3.
25. Salter M, Pogson CI. The role of haem in the regulation of rat liver tryptophan metabolism. *Biochem J* **1986**;240(1):259-63.
26. Lewis-Ballester A, Forouhar F, Kim SM, Lew S, Wang Y, Karkashon S*, et al.* Molecular basis for catalysis and substrate-mediated cellular stabilization of human tryptophan 2,3-dioxygenase. *Sci Rep* **2016**;6:35169.
27. Suzuki S, Tone S, Takikawa O, Kubo T, Kohno I, Minatogawa Y. Expression of indoleamine 2,3-dioxygenase and tryptophan 2,3-dioxygenase in early concepti. *Biochem J* **2001**;355(Pt 2):425-9.
28. Tatsumi K, Higuchi T, Fujiwara H, Nakayama T, Egawa H, Itoh K*, et al.* Induction of tryptophan 2,3-dioxygenase in the mouse endometrium during implantation. *Biochem Biophys Res Commun* **2000**;274(1):166-70.
29. Li DD, Gao YJ, Tian XC, Yang ZQ, Cao H, Zhang QL*, et al.* Differential expression and regulation of Tdo2 during mouse decidualization. *J Endocrinol* **2014**;220(1):73-83.
30. Yu CP, Pan ZZ, Luo DY. TDO as a therapeutic target in brain diseases. *Metab Brain Dis* **2016**;31(4):737-47.
31. Pilotte L, Larrieu P, Stroobant V, Colau D, Dolusic E, Frederick R*, et al.* Reversal of tumoral immune resistance by inhibition of tryptophan 2,3-dioxygenase. *Proc Natl Acad Sci U S A* **2012**;109(7):2497-502.
32. Dolusic E, Larrieu P, Moineaux L, Stroobant V, Pilotte L, Colau D*, et al.* Tryptophan 2,3-dioxygenase (TDO) inhibitors. 3-(2-(pyridyl)ethenyl)indoles as potential anticancer immunomodulators. *J Med Chem* **2011**;54(15):5320-34.
33. Nizet Y, Gillet L, Schroeder H, Lecuivre C, Louahed J, Renauld JC*, et al.* Antibody production by injection of living cells expressing non self antigens as cell surface type II transmembrane fusion protein. *J Immunol Methods* **2011**;367(1-2):70-7.
34. Van Pel A, De Plaen E, Boon T. Selection of highly transfectable variant from mouse mastocytoma P815. *Somat Cell Mol Genet* **1985**;11(5):467-75.
35. De Bock K, De Smet F, Leite De Oliveira R, Anthonis K, Carmeliet P. Endothelial oxygen sensors regulate tumor vessel abnormalization by instructing phalanx endothelial cells. *J Mol Med (Berl)* **2009**;87(6):561-9.
36. Nagy JA, Chang SH, Dvorak AM, Dvorak HF. Why are tumour blood vessels abnormal and why is it important to know? *Br J Cancer* **2009**;100(6):865-9.
37. Schramme F, Crosignani S, Frederix K, Hoffmann D, Stroobant V, Preillon J*, et al.* Inhibition of tryptophan-dioxygenase activity increases the anti-tumour efficacy of immune checkpoint inhibitors. *Cancer Immunol Res* **2019**;co-submitted.
38. Han S, Zhang C, Li Q, Dong J, Liu Y, Huang Y*, et al.* Tumour-infiltrating CD4(+) and CD8(+) lymphocytes as predictors of clinical outcome in glioma. *Br J Cancer* **2014**;110(10):2560-8.
39. Banerjee T, Duhadaway JB, Gaspari P, Sutanto-Ward E, Munn DH, Mellor AL*, et al.* A key in vivo antitumor mechanism of action of natural product-based brassinins is inhibition of indoleamine 2,3-dioxygenase. *Oncogene* **2008**;27(20):2851-7.
40. Muller AJ, DuHadaway JB, Jaller D, Curtis P, Metz R, Prendergast GC. Immunotherapeutic suppression of indoleamine 2,3-dioxygenase and tumor growth with ethyl pyruvate. *Cancer Res* **2010**;70(5):1845-53.

41. Godin-Ethier J, Hanafi LA, Piccirillo CA, Lapointe R. Indoleamine 2,3-dioxygenase expression in human cancers: clinical and immunologic perspectives. *Clin Cancer Res* **2011**;17(22):6985-91.
42. Schmidt SK, Muller A, Heseler K, Woite C, Spekker K, MacKenzie CR*, et al.* Antimicrobial and immunoregulatory properties of human tryptophan 2,3-dioxygenase. *Eur J Immunol* **2009**;39(10):2755-64.
43. Bessede A, Gargaro M, Pallotta MT, Matino D, Servillo G, Brunacci C*, et al.* Aryl hydrocarbon receptor control of a disease tolerance defence pathway. *Nature* **2014**;511(7508):184-90.
44. Xu F, Jin T, Zhu Y, Dai C. Immune checkpoint therapy in liver cancer. *J Exp Clin Cancer Res* **2018**;37(1):110.
45. Finkelmeier F, Waidmann O, Trojan J. Nivolumab for the treatment of hepatocellular carcinoma. *Expert Rev Anticancer Ther* **2018**;18(12):1169-75.
46. Salter M, Hazelwood R, Pogson CI, Iyer R, Madge DJ. The effects of a novel and selective inhibitor of tryptophan 2,3-dioxygenase on tryptophan and serotonin metabolism in the rat. *Biochem Pharmacol* **1995**;49(10):1435-42.
47. Bose A, Barik S, Banerjee S, Ghosh T, Mallick A, Bhattacharyya Majumdar S*, et al.* Tumor-derived vascular pericytes anergize Th cells. *J Immunol* **2013**;191(2):971-81.
48. Ochs K, Sahm F, Opitz CA, Lanz TV, Oezen I, Couraud PO*, et al.* Immature mesenchymal stem cell-like pericytes as mediators of immunosuppression in human malignant glioma. *J Neuroimmunol* **2013**;265(1-2):106-16.
49. Wang Y, Liu H, McKenzie G, Witting PK, Stasch JP, Hahn M*, et al.* Kynurenine is an endothelium-derived relaxing factor produced during inflammation. *Nat Med* **2010**;16(3):279-85.
50. Tattevin P, Monnier D, Tribut O, Dulong J, Bescher N, Mourcin F*, et al.* Enhanced indoleamine 2,3-dioxygenase activity in patients with severe sepsis and septic shock. *J Infect Dis* **2010**;201(6):956-66.
51. Stanley CP, Maghzal GJ, Ayer A, Talib J, Giltrap AM, Shengule S*, et al.* Singlet molecular oxygen regulates vascular tone and blood pressure in inflammation. *Nature* **2019**;566(7745):548-52.
52. Germeyer A, Sharkey AM, Prasadajudio M, Sherwin R, Moffett A, Bieback K*, et al.* Paracrine effects of uterine leucocytes on gene expression of human uterine stromal fibroblasts. *Mol Hum Reprod* **2009**;15(1):39-48.
53. Hsu YL, Hung JY, Chiang SY, Jian SF, Wu CY, Lin YS*, et al.* Lung cancer-derived galectin-1 contributes to cancer associated fibroblast-mediated cancer progression and immune suppression through TDO2/kynurenine axis. *Oncotarget* **2016**;7(19):27584-98.

676 **Table 1: IHC Antibodies**
677

Primary antibodies				
Species	**Antigen**	**Clone**	**Reference**	**Dilution**
Rabbit	CA9	polyclonal	NovusBio (#NB100-417)	1:1000
Rabbit	CD3	SP7	Abcam (#ab16669)	1:500
Rabbit	CD8	SP16	ThermoFisher Scientific (#MA5-14548)	1:200
Rabbit	CD34	EP373Y	GeneTex (#GTX61737)	1:1000
Mouse	CD68	PG-M1	ThermoFisher Scientific (#MA5-12407)	1:50
Mouse	Cytokeratin	AE1/AE3	Dako (#M3515)	1:50
Rat	GFAP	2.2B10	Invitrogen (#13-0300)	1:50
Mouse	HLA-DR	LN-3	Novocastra (#NCL-LN3)	1:100
Mouse	IDO1	4.16H1	Theate et al, 2015 (13)	0.5µg/ml
Rabbit	Ki67	SP6	ThermoFisher Scientific (#RM9106)	1:200
Rabbit	PDGFRβ	Y92	Abcam (#ab32570)	1:200
Rabbit	αSMA	EPR5368	Merck (#MABT381)	1:2000
Mouse	TDO	III	iTeos Therapeutics	0.5 µg/ml
Mouse	TDO	V	iTeos Therapeutics	0.5 µg/ml
Rabbit	β3-tubulin	TUJ1	Cell Signaling (#5666)	1:100
Mouse IgG2a, κ isotype ctrl		MOPC173	BioLegend (#400209)	0.5 µg/ml
Secondary antibodies				
EnVision+ HRP goat anti-mouse			Dako (#K4001)	/
EnVision+ HRP goat anti-rabbit			Dako (#K4003)	/
ImmPRESS HRP goat anti-rat			Vector (#MP-7444)	/
Tyramide reagents				
Alexa Fluor	**Used to stain**		**Reference**	**Dilution**
488	CA9, CD3, HLA-DR, PDGFRβ, αSMA		ThermoFisher Scientific (#B40953)	1:50
555	CD8, CD34, β3-tubulin		ThermoFisher Scientific (#B40955)	1:50
594	CD68, GFAP, Ki67, cytokeratin		ThermoFisher Scientific (#B40957)	1:50
647	TDO		ThermoFisher Scientific (#B40958)	1:50

678

679 **Table 2**. **TDO protein expression in human tumors**
680

Tumors	TDO+/tot	%	Level 0	Level 1	Level 2	Level 3
Hepatocarcinoma	10/10	100%	0	0	0	10
Glioblastoma	38/39	97%	1	4	9	25
Bladder carcinoma	12/13	92%	1	2	7	3
Pancreatic carcinoma	10/11	91%	1	7	2	1
Colon carcinoma	9/10	90%	1	4	4	1
Stomach carcinoma	6/8	75%	2	2	4	0
Endometrial carcinoma	5/7	71%	2	5	0	0
Lung carcinoma	7/11	64%	4	1	5	1
Melanoma	3/6	50%	3	0	1	2
Corresponding metastatic lymph nodes	8/9	89%	1	2	3	3
Corresponding non-metastatic lymph nodes	1/9	11%	8	1	0	0
Breast carcinoma	4/9	44%	5	4	0	0
Corresponding infiltrated lymph nodes	12/15	80%	3	9	3	0
Corresponding non-infiltrated lymph nodes	0/6	0%	6	0	0	0
Kidney carcinoma	4/10	40%	6	3	0	1
Astrocytoma	0/12	0%	12	0	0	0
All tumors (without lymph nodes)	108/146	74%				

681
682 The table lists all cancer types tested, the number and percentage of samples containing TDO-positive
683 cells as well as the level of TDO expression (illustrated in Fig. 1). We performed the screening by staining
684 three adjacent tissue sections with the anti-TDO mAb III, mAb V and with an isotype control. The two
685 following sections were used for RNA extraction and RT-qPCR analyses to confirm that tissues showing
686 staining by IHC also contained *TDO2* mRNA. When IHC staining was present but no mRNA was
687 detected by RT-qPCR, the mRNA of the house-keeping gene EF1 was often highly degraded. If, on the
688 contrary, EF1 mRNA was in a normal range, we performed ISH to confirm the IHC staining. In cases
689 with a positive RT-qPCR result, but a negative IHC result, we suspected contamination of the mRNA
690 when cutting the tissues on the microtome. To confirm the IHC result, we performed ISH on those
691 tissues. In some cases, especially in lung and kidney samples, we detected *TDO2* by ISH, showing that
692 the positive RT-qPCR result was correct, but the expression of the TDO protein probably too low to be
693 detected by the antibody. A tumor was considered positive when IHC staining was detected. We did not
694 take into account tumors that were positive by RT-qPCR, but negative in IHC because we knew from *in*
695 *vitro* experiments that cell lines displaying the same expression and staining pattern did not have any
696 catalytic activity.

Table 3. TDO expression in non-tumoral lung pericytes

Clinical characteristics	TDO level	Inflammation	Granulation tissue
Normal lung (autopsy after sudden death)	0	/	/
Non malignant lung (atelectasis)	0	/	/
Distant metastasis (colorectal adenocarcinoma)	0	/	/
Distant metastasis (sarcoma)	0	/	/
Distant metastasis (sarcoma)	0	/	/
Distant metastasis (sarcoma)	0	/	/
Normal lung (negative search for metastases)	1	some cells	/
Non malignant lung (atelectasis and cyst)	1	some cells	/
Malignant lung carcinoma	1	Yes	/
Non malignant lung (emphysema)	1	Yes	/
Distant metastasis (sarcoma)	2	Yes	Yes
Malignant carcinoid tumor	2	Yes	Yes
Malignant lung carcinoma	3	Yes	/

The table lists all lung samples resected at distant sites from the indicated lesion, the level of TDO expression and the presence of inflammation or granulation tissue (illustrated in Fig. 4). The staining protocol is the same as in Table 2. We observed that TDO was exclusively expressed by pericytes.

Legends

Figure 1. TDO expression in human tumors

(**A**) Representative pictures showing TDO IHC staining with the mouse anti-TDO mAb V on FFPE sections of different human tumors. The dotted lines delineate necrotic or hemorrhagic tumor areas. Scale bars = 50-2,000 µm.

(**B**) TDO was stained by IHC with the mouse anti-TDO mAb V and mAb III, and by ISH with anti-h*TDO2* mRNA probes on adjacent sections of an FFPE kidney carcinoma. Scale bar = 50 µm.

(**C**) Representative pictures illustrating different TDO expression levels: level 0 is negative for TDO, level 1 contains some isolated TDO-positive cells, level 2 contains regions enriched in TDO-positive cells and level 3 contains several regions with high amounts of TDO-positive cells. Scale bar = 50 µm. The graph and the cross-tabulation represent the numbers and percentages of tumors organized according to the level of TDO expression and the tumor grade.

For all IHC stainings, negative controls were performed with a mouse IgG2a isotype control. ISH negative controls were performed with an anti-dapB probe. All negative controls remained unstained.

Figure 2. TDO expression by pericytes in abnormal tumor vessels

(**A**) Co-stainings were performed by immunofluorescence as indicated on FFPE glioblastoma sections, with TDO mAb V in orange and the co-markers in green. Co-localization appears in yellow. Orange arrows point TDO-positive cells, green arrows point cells labelled with co-markers, and yellow arrows point cells where TDO co-localizes with one of the cell type markers. Scale bars = 50 µm.

(**B**) Triple immunofluorescence co-staining of glioblastoma sections for TDO mAb V (orange), PDGFRβ (green) and CD34 (purple). Co-localization of TDO with PDGFRβ is represented in yellow. Scale bars = 20 µm.

(**C**) Immunofluorescence co-staining for TDO mAb V (orange) and CA9 (green) on a glioblastoma section. The dotted line delineates the necrotic tumor area. Scale bar = 100 µm. For all IF stainings, negative controls were performed by omitting the primary antibody and remained unstained.

Figure 3. Quantification of T lymphocytes in TDO-positive and TDO-negative glioblastoma areas

Immunofluorescence co-stainings were performed for TDO mAb V, CD3, CD8 and Ki67 on tissue sections from 29 glioblastomas multiforme. Negative controls were performed by omitting the primary antibody and remained unstained. Infiltrating lymphocytes were counted in zones 60 µm away from TDO-positive cells and compared to lymphocytes in the remaining tumor regions (the quantification workflow is illustrated in Fig. S4). (**A**) $CD3^+$, $CD3^+CD8^-$ or $CD3^+CD8^+$ cells were counted and expressed as number of cells per mm^2 of tissue area (mean±SD, Wilcoxon matched-pairs signed rank test). (**B**) Ki67-positive lymphocytes were counted and expressed as percentage of the parental lymphocyte population (mean±SD, Wilcoxon matched-pairs signed rank test).

Figure 4. TDO expression in human normal liver, pulmonary granulomas and placental tissues

(**A**) Representative pictures showing anti-TDO mAb V staining of FFPE sections of liver, lung, decidua and ectopic pregnancies. Scale bars = 50-2000 µm. Similar stainings were observed with both primary antibodies mAb III and V. Negative controls were performed with a mouse IgG2a isotype control and remained unstained.

(**B**) Co-staining of pulmonary granulomas and ectopic pregnancies for TDO mAb V (orange), PDGFRβ (green), CD34 (purple), cytokeratin (blue) or CD68 (macrophages, blue). Co-localization of TDO with PDGFRβ is represented in yellow. Co-localization of TDO with cytokeratin is represented in clear blue. The arrows point a pericyte that co-expresses TDO and PDGFRβ. The surrounded cell is a syncytiotrophoblast that expresses both TDO and

cytokeratin. Scale bars = 20-50 μm. Negative controls were performed by omitting the primary antibody and remained unstained.

Figure 1

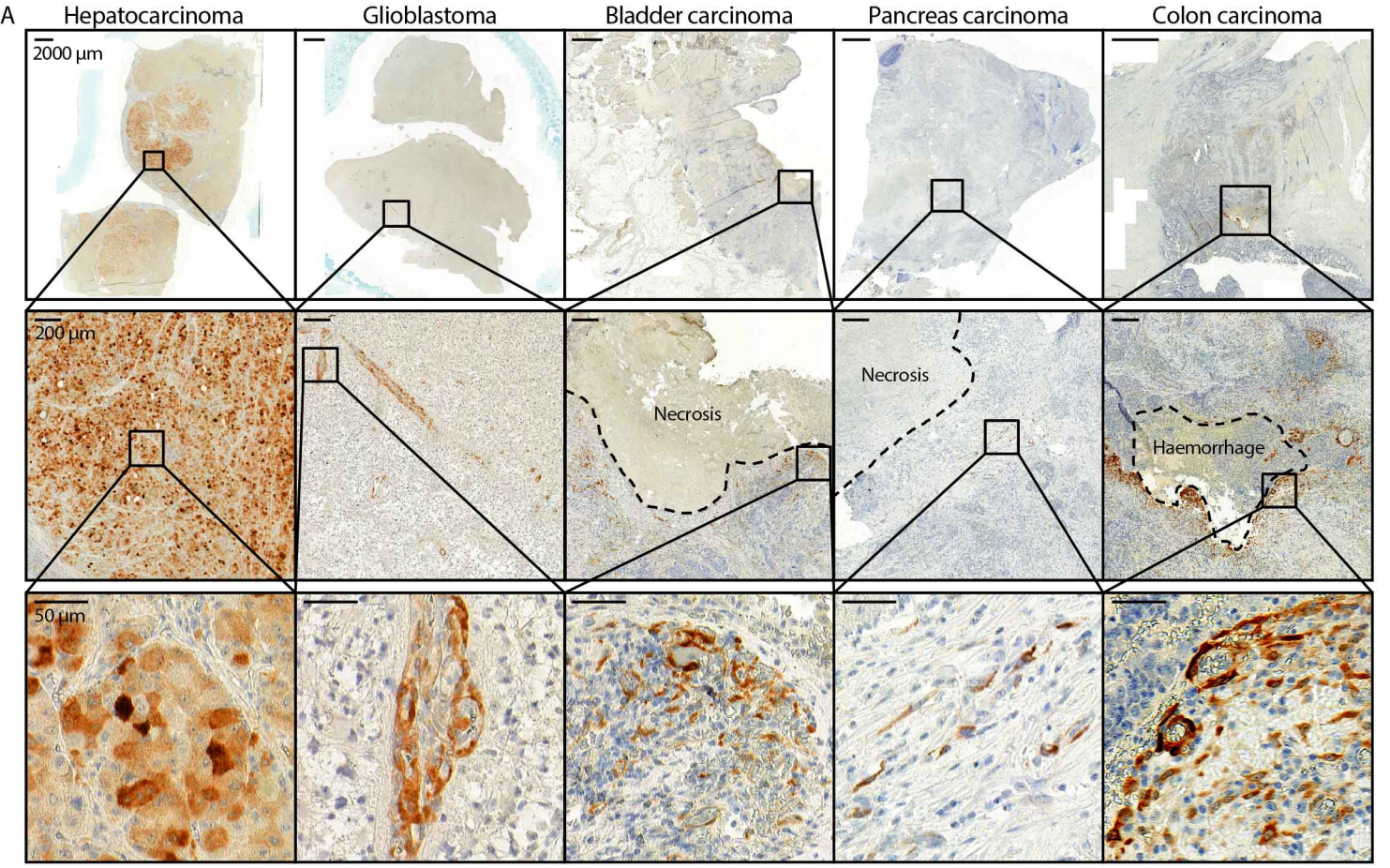

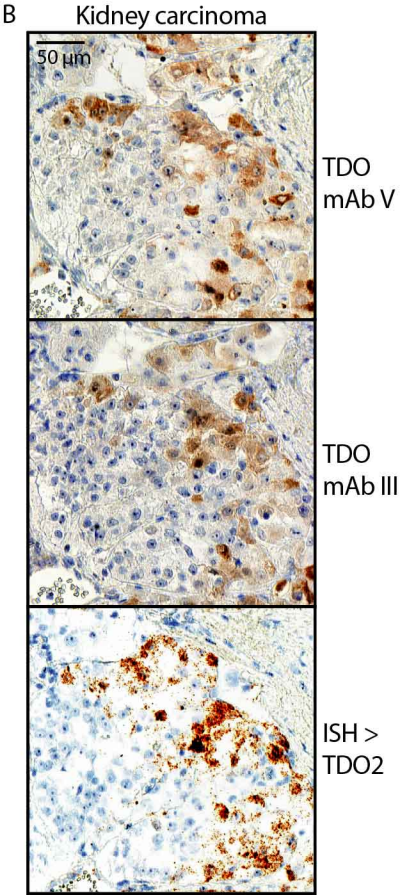

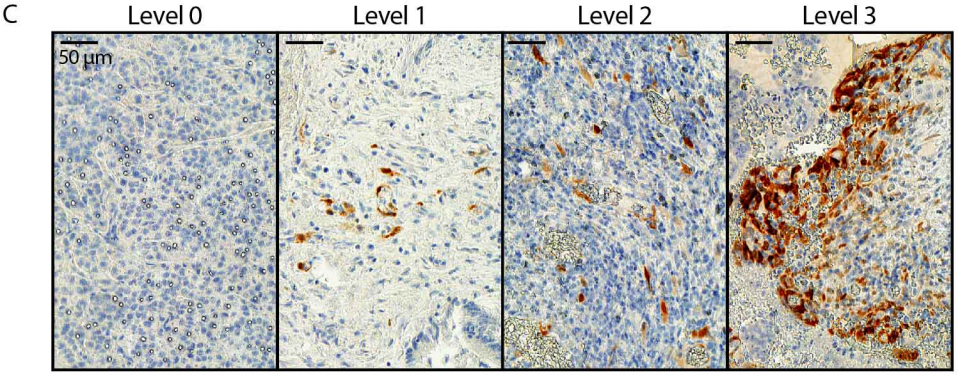

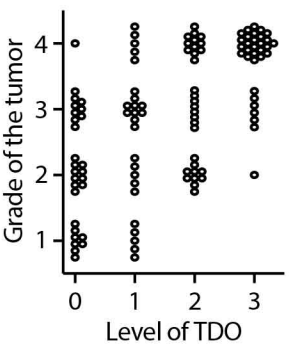

			Level of TDO				Total
			0	1	2	3	
Grade of the tumor	4	#	1	5	12	25	43
		%	0.9%	4.3%	10.4%	21.7%	37.4%
	3	#	9	10	8	6	33
		%	7.8%	8.7%	7.0%	5.2%	28.7%
	2	#	10	5	10	1	26
		%	8.7%	4.3%	8.7%	0.9%	22.6%
	1	#	8	5	0	0	13
		%	7.0%	4.3%	0.0%	0.0%	11.3%
Total		#	28	25	30	32	115
		%	24.3%	21.7%	26.1	27.8%	100%

Spearman correlation coefficient = 0.6115
p-value = <0.0001

Figure 2

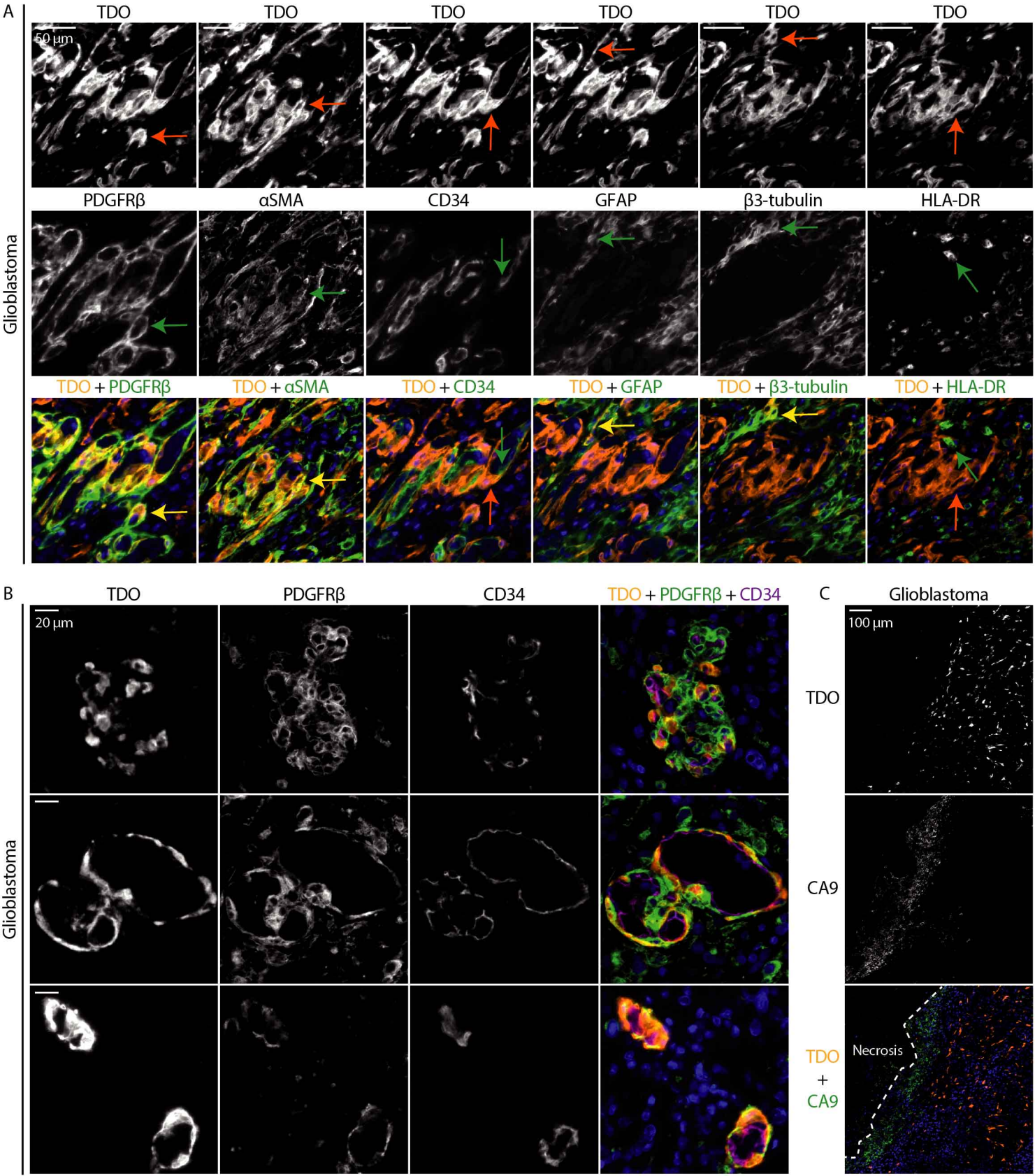
A
TDO
TDO
TDO
TDO
TDO
TDO
50 µm
PDGFRβ
αSMA
CD34
GFAP
β3-tubulin
HLA-DR
Glioblastoma
TDO + PDGFRβ
TDO + αSMA
TDO + CD34
TDO + GFAP
TDO + β3-tubulin
TDO + HLA-DR
B
TDO
PDGFRβ
CD34
TDO + PDGFRβ + CD34
20 µm
Glioblastoma
C
Glioblastoma
100 µm
TDO
CA9
TDO
+
CA9
Necrosis

Figure 3

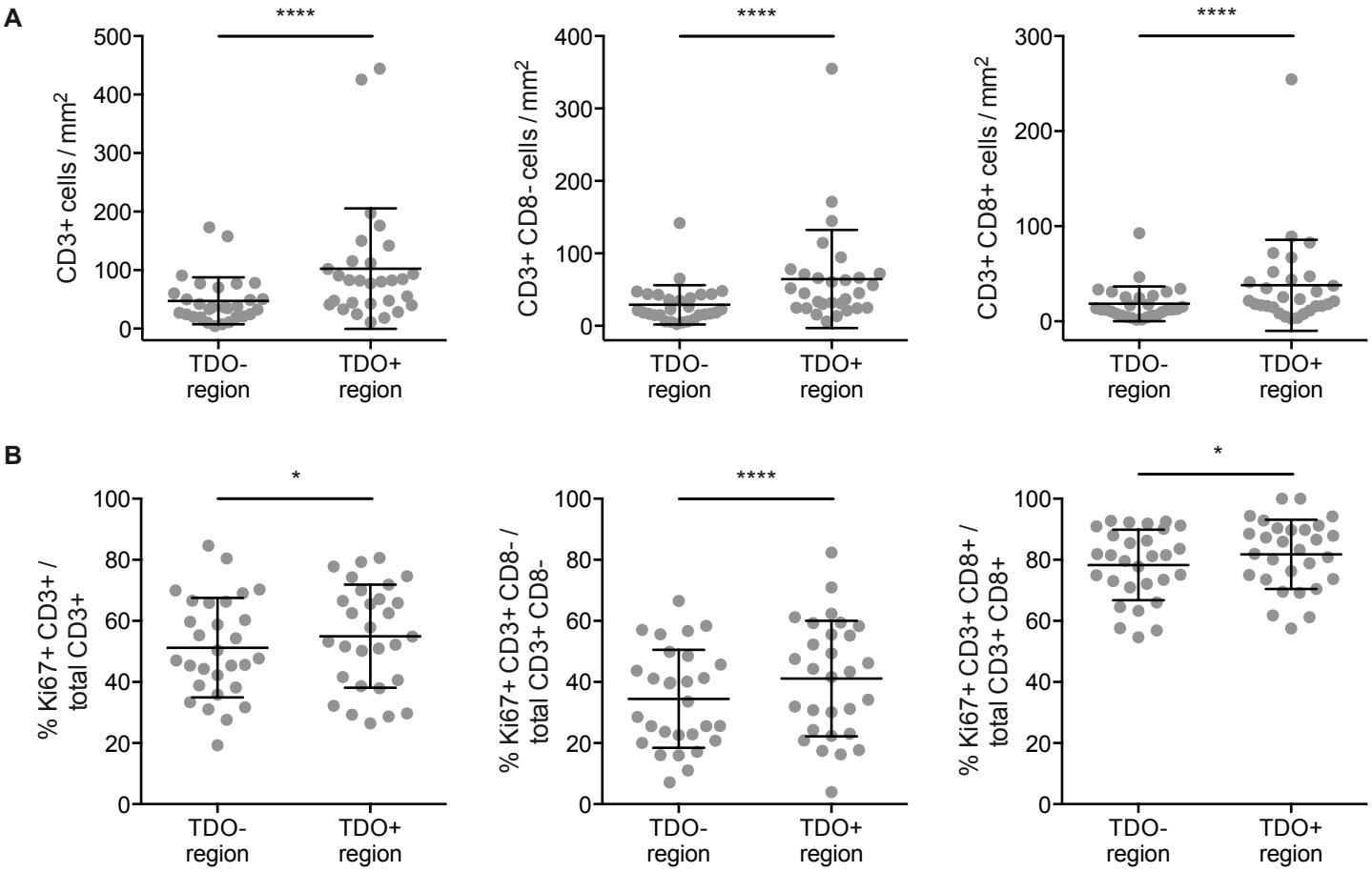
A
****
CD3+ cells / mm2
500
400
300
200
100
0
TDO-
region
TDO+
region
****
CD3+ CD8- cells / mm2
400
300
200
100
0
TDO-
region
TDO+
region
****
CD3+ CD8+ cells / mm2
300
200
100
0
TDO-
region
TDO+
region
B
*
% Ki67+ CD3+ /
total CD3+
100
80
60
40
20
0
TDO-
region
TDO+
region
****
% Ki67+ CD3+ CD8- /
total CD3+ CD8-
100
80
60
40
20
0
TDO-
region
TDO+
region
*
% Ki67+ CD3+ CD8+ /
total CD3+ CD8+
100
80
60
40
20
0
TDO-
region
TDO+
region

Figure 4

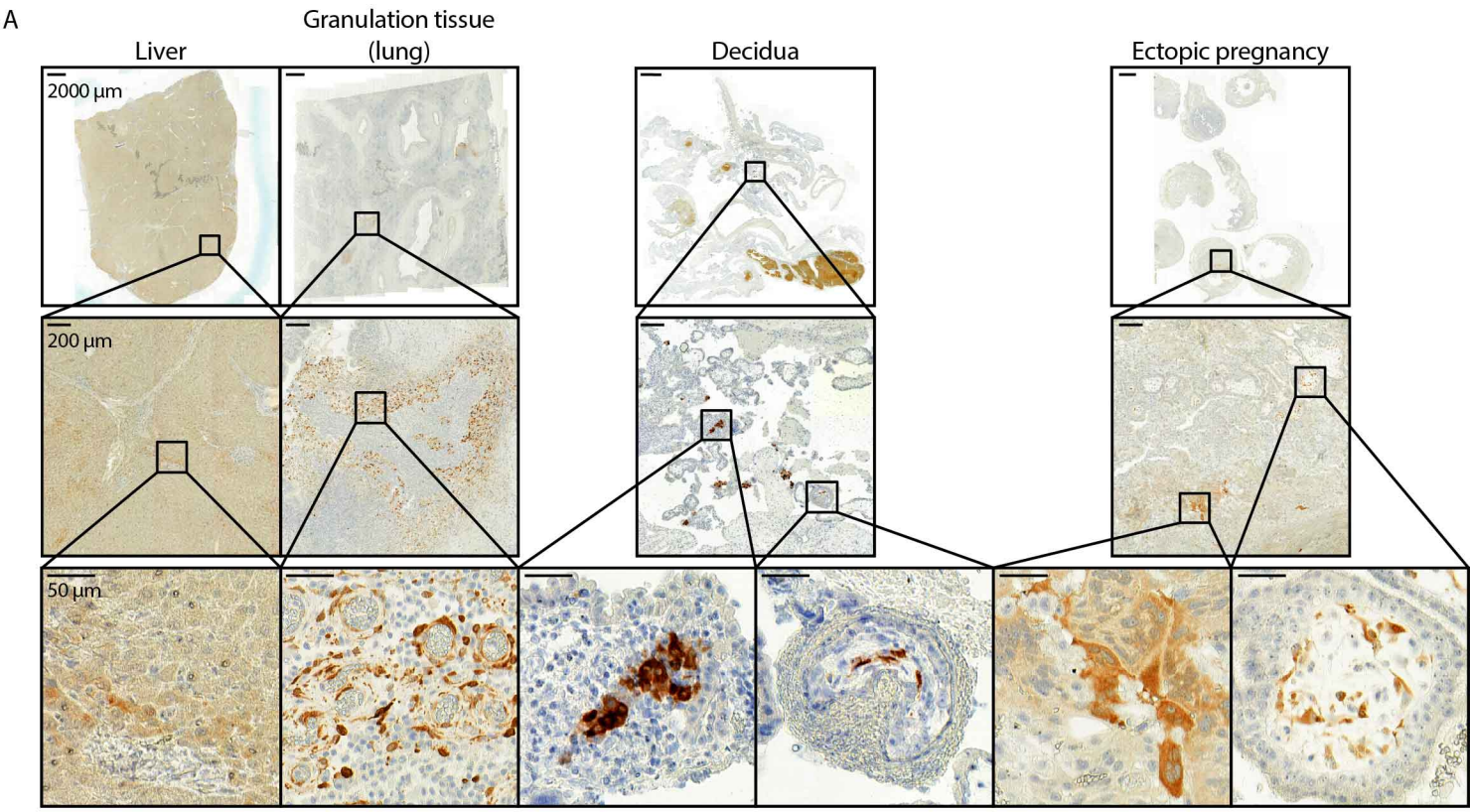
A
Liver
Granulation tissue (lung)
Decidua
Ectopic pregnancy
2000 µm
200 µm
50 µm

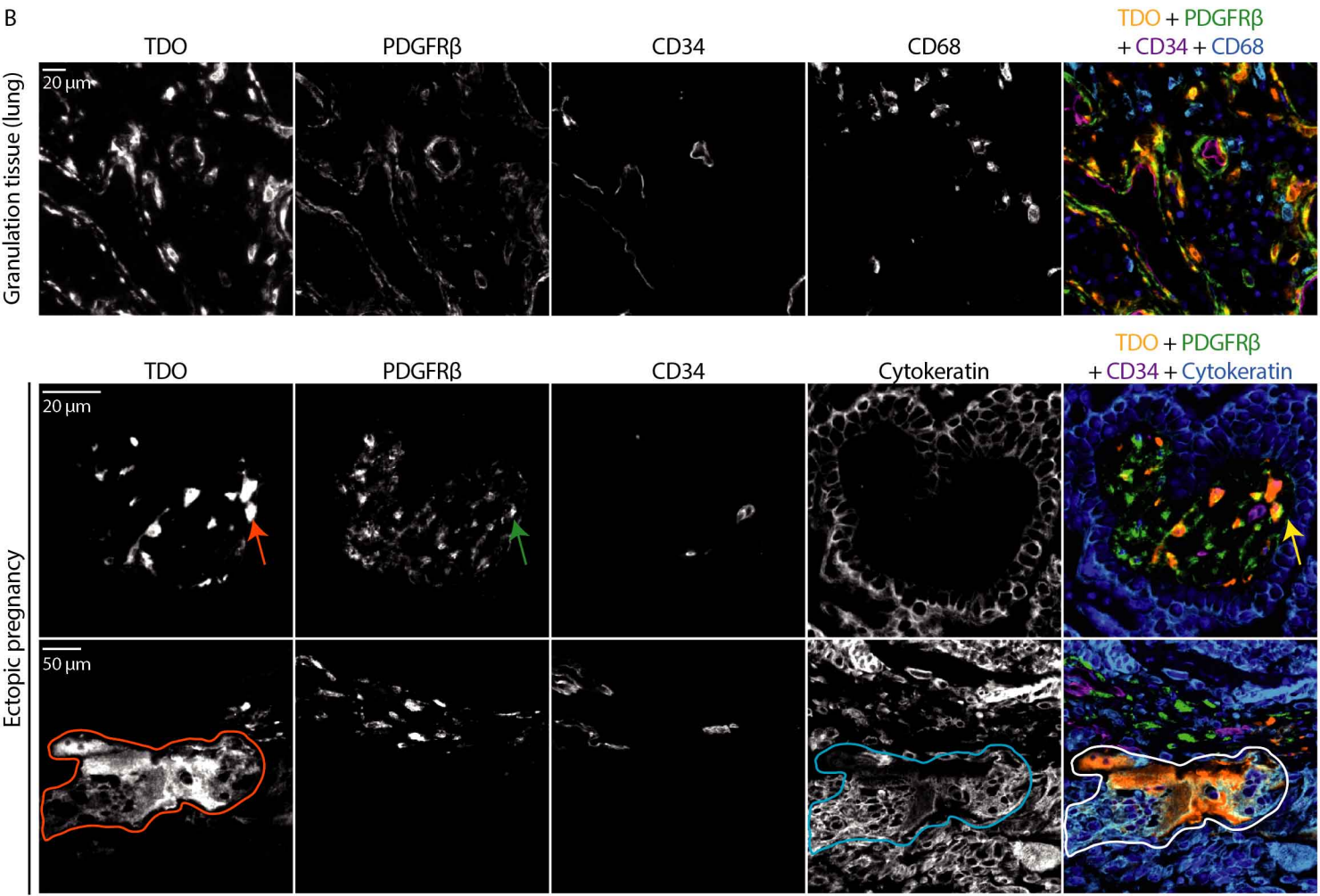
B
TDO
PDGFRβ
CD34
CD68
TDO + PDGFRβ + CD34 + CD68
Granulation tissue (lung)
20 µm
TDO
PDGFRβ
CD34
Cytokeratin
TDO + PDGFRβ + CD34 + Cytokeratin
Ectopic pregnancy
20 µm
50 µm